Oxygen Permeability and Structural Stability of a Novel Tantalum-Doped Perovskite $BaCo_{0.7}Fe_{0.2}Ta_{0.1}O_{3-\delta}$

Huixia Luo, Bingbing Tian, Yanying Wei, and Haihui Wang
School of Chemistry and Chemical Engineering, South China University of Technology, Guangzhou 510640, China

Heqing Jiang and Jürgen Caro
Institute of Physical Chemistry and Electrochemistry, Leibniz University of Hannover, Hannover D-30167, Germany

DOI 10.1002/aic.12044
Published online August 24, 2009 in Wiley InterScience (www.interscience.wiley.com).

Dense $BaCo_{0.7}Fe_{0.2}Ta_{0.1}O_{3-\delta}$ (BCFT) perovskite membranes were successfully synthesized by a simple solid state reaction. In situ high-temperature X-ray diffraction indicated the good structure stability and phase reversibility of BCFT at high temperatures. The thermal expansion coefficient (TEC) of BCFT was determined to amount 1.02 $\times$ 10^{-5} K^{-1}, which is smaller than those of $Ba_{0.5}Sr_{0.5}Co_{0.8}Fe_{0.2}O_{3-\delta}$ (BSCF) (1.15 $\times$ 10^{-5} K^{-1}), $SrCo_{0.8}Fe_{0.2}O_{3-\delta}$ (SCF) (1.79 $\times$ 10^{-5} K^{-1}), and $BaCo_{0.4}Fe_{0.4}Zr_{0.2}O_{3-\delta}$ (BCFZ) (1.03 $\times$ 10^{-5} K^{-1}). It can be seen that the introduction of Ta ions into the perovskite framework could effectively lower the TEC. Thickness dependence studies of oxygen permeation through the BCFT membrane indicated that the oxygen permeation process was controlled by bulk diffusion. A membrane reactor made from BCFT was successfully operated for the partial oxidation of methane to syngas at 900°C for 400 h without failure and with the relatively high, stable oxygen permeation flux of about 16.8 ml/min cm^2. *AIChE J,* 56: 604–610, 2010
Keywords: perovskite, oxygen separation, mixed conductor, membrane, POM

Introduction

In recent years, mixed-conducting ceramic oxides with oxygen ionic and electronic conductivity have attracted increasing attention due to the potential applications in oxygen separation from air,[1–9] in the partial oxidation of methane (POM) to syngas,[10–16] in the selective oxidation of hydrocarbons,[17–19] for the power plants with carbon dioxide sequestration.[20,21] Especially, the promising application in the POM to synthesis gas (a H_2:CO mixture 2:1) seems to be an attractive route for upgrading natural gas. Promising membranes should not only possess high-oxygen permeability but also good structural stability to withstand the harsh working conditions, such as the reducing atmosphere of synthesis gas or steam. During the last 10 years, much progress was achieved to meet the aforementioned requirements. $SrCo_{0.8}Fe_{0.2}O_{3-\delta}$ (SCF) possesses high-oxygen permeability, and the oxygen permeation fluxes can reach 3.1 ml/min cm^2 under an air/He oxygen gradient at 850°C with 1.0 mm membrane thickness.[22] Unfortunately, SCF shows low-structural stability in a reducing atmosphere. To improve the structural stability, many researchers doped SCF with higher valence metal ions such as: A = Ba^{2+}, La^{2+}, Ca^{2+}, B = Ti^{4+}, Zr^{4+}, Nb^{5+}. Yang's group[23–27] developed a series of materials based on $BaTi_{0.2}Co_{0.5}Fe_{0.3}O_{3-\delta}$ (BTCF) and $BaCo_{0.4}Fe_{0.4}Zr_{0.2}O_{3-\delta}$ (BCFZ). By partially substituting Ba by Sr, a novel material named $Ba_{0.5}Sr_{0.5}Co_{0.8}Fe_{0.2}O_{3-\delta}$ (BSCF), which shows high-oxygen permeability and good

Correspondence concerning this article should be addressed to H. Wang at hhwang@scut.edu.cn

operation stability in the POM reaction, was developed.[23,24] ZrO_2 or YSZ-doped SCF had been proven to have a high-oxygen permeation flux, stable lattice structure, and high-mechanical strength,[28] although a potential problem of the thermal mismatch between two phases in SCF were not solved yet. To further improve the stability of the membrane materials, cations with constant valence (Zr^{4+}, Ga^{3+}, and Al^{3+}) were used to partially substitute the reducible B-site ions (Co^{4+}/Co^{3+} and Fe^{4+}/Fe^{3+}).[29–32] However, some researchers found that the pure-phase perovskite was hard to obtain as the large ions (such as Zr) were not easy to bring into the perovskite structure due to the large ionic radius.[9,26,32] To prepare a pure-phase pervoskite structure, some ions with small size were used. For example, Wang et al.[33] found that Zn can be easily brought into the perovskite structure and developed a $Ba_{0.5}Sr_{0.5}Fe_{0.8}Zn_{0.2}O_{3-\delta}$ membrane, which shows a high-oxygen permeation flux and an excellent phase stability under low-oxygen partial pressure. Recently, a novel perovskite-type mixed-conducting membrane based on $SrSc_{0.05}Co_{0.95}O_{3-\delta}$ with good oxygen permeability was reported.[34,35] However, Sc is a very expensive metal, which might limit the application of this material.

Nagai et al.[36] found that Nb is the best candidate for the cation substitution of $SrCo_{1-x}M_xO_{3-\delta}$. Shao et al.[37] found that the substitution of Ba for Sr on the A-site can prevent the long range ordering of oxygen vacancies, thus improving the stability of the perovskite. Subsequently, a novel perovskite of the composition $BaCo_{0.7}Fe_{0.2}Nb_{0.1}O_{3-\delta}$ was developed, and it was found that $BaCo_{0.7}Fe_{0.2}Nb_{0.1}O_{3-\delta}$ exhibits a high-oxygen permeability and good phase stability.[38,39] In this article, Ta was chosen for the substitution on the B-site, because Ta is the same group element as Nb and, furthermore, the thermal expansion coefficient (TEC) of Ta_2O_5 (6.6×10^{-6} K^{-1}) is lower than that of Nb_2O_5 (7.07×10^{-6} K^{-1}). Therefore, we can expect that the incorporation of the pentavalent Ta^{5+} ion in the perovskite structure can lower the TEC and improve the stability. The perovskite $BaCo_{0.7}Fe_{0.2}Ta_{0.1}O_{3-\delta}$ (BCFT) was synthesized by a solid state reaction. The phase structure and the oxygen permeability under air/He gradient and POM reaction were investigated. The rate-limiting step for the oxygen transport was clarified and the operation stability was studied.

Experimental

The BCFT powder samples were synthesized using a solid state reaction. $BaCO_3$, Co_2O_3, Fe_2O_3, and Ta_2O_5 (all reagents with A.R. purity) were weighted according to their stoichiometry and mixed in an agate mortar for 1.5 h and then ball-milled for 24 h in ethanol. Then, the mixtures were calcined at 950°C for 10 h with heating and cooling rates of 2°C/min. Then, the primary powders were mixed finely in an agate mortar and sintered at 950°C for 10 h again, with the same heating and cooling rates as in the first calcination.

The as-synthesized powders were pressed to disk membranes under a pressure of 18–24 MPa in a stainless steel module with a diameter of 16 mm. The green disks were sintered at 1000°C for 10 h. The densities of the sintered membranes were determined by the Archimedes method using ethanol. Only those membranes that had relative densities higher than 95% were chosen for the oxygen permeation studies.

The crystal structures and lattice constant of the BCFT perovskite were characterized by *in situ* high-temperature X-ray diffraction (XRD) (PHILIPS-PW1710) using Cu Kα radiation. The sample was tested in a high-temperature cell (Bühler HDK 2.4 with REP 2000) with a heated Pt sample holder upto 1000°C in different atmospheres (air, 2% O_2 in Ar, and pure Ar). The Pt heater was used as the sample holder and a thermal coupler was connected directly on the Pt heater (i.e., sample holder). The heating and cooling rates amounted to 5°C/min. At each temperature step, the temperature was held for 70 min. Data were collected in a continuous scan mode in the range of 20°–80° with intervals of 0.05°. The peaks of Pt were used as an internal standard to calculate the lattice constant of the BCFT perovskite. The element analysis of fresh and spent membranes was performed by energy dispersive X-ray spectroscopy (SEM-EDXS, Jeol-JSM-6700F).

Oxygen temperature-programmed desorption (O_2-TPD) was performed on a Micromeritics AutoChem 2920™. Before O_2 desorption, the samples (about 1.0 g, particle size = 40–60 mesh) were pretreated in flowing O_2 (99.999%, 30 ml/min) at 950°C for 2 h. Then, the temperature was cooled down to 40°C at a rate of 10°C/min, and O_2-TPD was performed from 50°C to 1000°C with a heating rate of 10°C/min, where He (99.999%, 30 ml/min) was used as the carrier gas. The amount of desorbed oxygen was detected by gas chromatography using a thermal conductivity detector. To investigate the reversibility of oxygen adsorption and desorption, after O_2-TPD, the samples were pretreated again under flowing O_2 at 950°C, and then the next O_2-TPD run was performed again. After the last run, the samples were characterized by XRD.

The oxygen permeation was conducted on a self-made high-temperature oxygen permeation cell, as shown in Figure 1. The membrane was sealed on a quartz tube (Ø = 16 mm). Another quartz tube (Ø = 24 mm) served as the air side of the permeator. A tubular furnace was used to heat the permeator. The temperature was controlled by a microprocessor temperature controller (Model Al-708, Xiamen Yudian Electronics Technology Research Institute, China) within ±1°C of the set points and monitored by a K-type thermocouple positioned near the discs. A gold paste from the Institute of Platinum Manufactory (Guizhou, China) was used as the binding agent to seal the disk onto a quartz tube at 950°C for 5 h. The inlet gas flow rates were controlled by mass flow controllers (model D07-7A/ZM, Beijing Jianzhong Machine Factory, China). Synthetic air was fed to the air side of the permeator and high-purity He (>99.995%) was fed to the sweep side of the permeator. A gas chromatograph (Shimadzu GC-14B) equipped with a TDX-01 column for the separation of oxygen and nitrogen was connected to the exit of the sweep side. The GC was frequently calibrated using standard gases like oxygen and helium to ensure reliability of the experimental data. The leakage of oxygen was subtracted when the oxygen permeation flux was calculated. Assuming that leakage of nitrogen and oxygen through pores or cracks is in accordance with Knudsen diffusion, the fluxes of leaked N_2 and O_2 are related by Eq. 1 as follows:

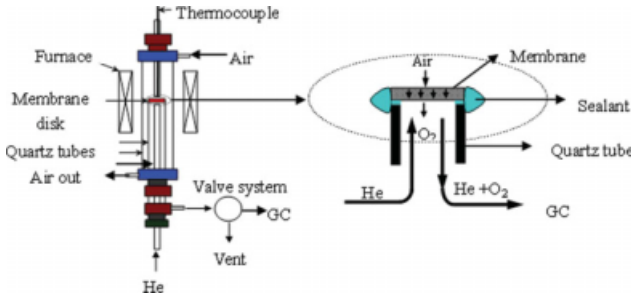

Figure 1. Permeation cell used for the oxygen permeation at high temperatures.

[Color figure can be viewed in the online issue, which is available at www.interscience.wiley.com.]

$$J_{N_2}^{Leak} : J_{O_2}^{Leak} = \sqrt{\frac{32}{28}} \times \frac{0.79}{0.21} = 4.02 \quad (1)$$

The oxygen permeation flux was then calculated as follows:

$$J_{O_2}\left(\text{ml/min}\cdot\text{cm}^2\right) = \left(C_{O_2} - \frac{C_{N_2}}{4.02}\right) \times \frac{f}{S} \quad (2)$$

where C_{O_2}, C_{N_2} are the oxygen and nitrogen concentrations calculated from GC calibration, f is the total flow rate of the outlet on the sweep side, which was measured by a soap film meter. S is the membrane area.

Results and Discussion

In situ XRD provides an effective and direct way to characterize the high-temperature structure changes during increasing and decreasing temperatures. Figure 2 shows the XRD patterns of BCFT in air for increasing temperature from 30°C to 1000°C indicating that BCFT remains in the perovskite structure over the examined temperature range. The XRD patterns during the temperature increase and decrease are identical. In turn, this means that BCFT exhibits good phase reversibility and structure stability in air at high temperatures, which can also be proven by the multirun O_2-TPD.

During the oxygen permeation experiments, one side of the membrane was exposed to synthetic air (high-oxygen partial pressure); the other side of the membrane was exposed to the sweep gases Ar or He (low-oxygen partial pressure). The proven phase stability of BCFT in air alone is not enough to recommend BCFT as a candidate for oxygen separation. Therefore, it is necessary to study the high-temperature phase stability of BCFT at low-oxygen partial pressure, e.g., 2% O_2 in Ar or pure Ar, as shown in Figure 3. The XRD patterns of BCFT powder at 900°C under different oxygen partial pressures show that BCFT can remain in its perovskite structure both in air and 2% O_2 in Ar, and even in pure Ar with an oxygen partial pressure $\leq 1 \times 10^{-5}$ bar. These results indicate that BCFT possesses an excellent phase stability at high temperatures not only in air but also in atmospheres with an oxygen partial pressure $\leq 1 \times 10^{-5}$ bar. In fact, the oxygen concentration at the sweep side during the oxygen permeation is around 1–3% above 800°C. Therefore, it is expected that a BCFT membrane can be steadily operated in the oxygen separation for a long time.

Figure 4 shows the lattice constants of BCFT at various temperatures determined from the XRD data in air. From Figure 4, it can be seen that the lattice constant increases linearly with temperatures for both increasing and decreasing temperatures. Within the temperature range studied, the change of the lattice constant of BCFT is 0.99%. The thermal expansion coefficient (TEC) was calculated following the definition $\frac{d(\Delta a/a_0)}{dT}$ (a, lattice constant; a_0, lattice constant at room temperature). From Figure 4, the average TEC of BCFT is found to be 1.02×10^{-5} K^{-1}. In our previous study,[40] by the same *in situ* high-temperature XRD, it was found that the TECs of BSCF, SCF, and BCFZ are 1.15×10^{-5} K^{-1}, 1.79×10^{-5} K^{-1}, and 1.03×10^{-5} K^{-1}, respectively. It can be seen that the TEC of BCFT is smaller than SCF and BCFS, and even slightly smaller than that of BCFZ. The lower TEC is beneficial for the operation stability of BCFT membrane.

The O_2-TPD technique provides not only an effective way to characterize the oxygen absorption/adsorption properties of the ceramic oxides but also an indirect evidence for the structure stability. Figure 5 presents the multirun O_2-TPD

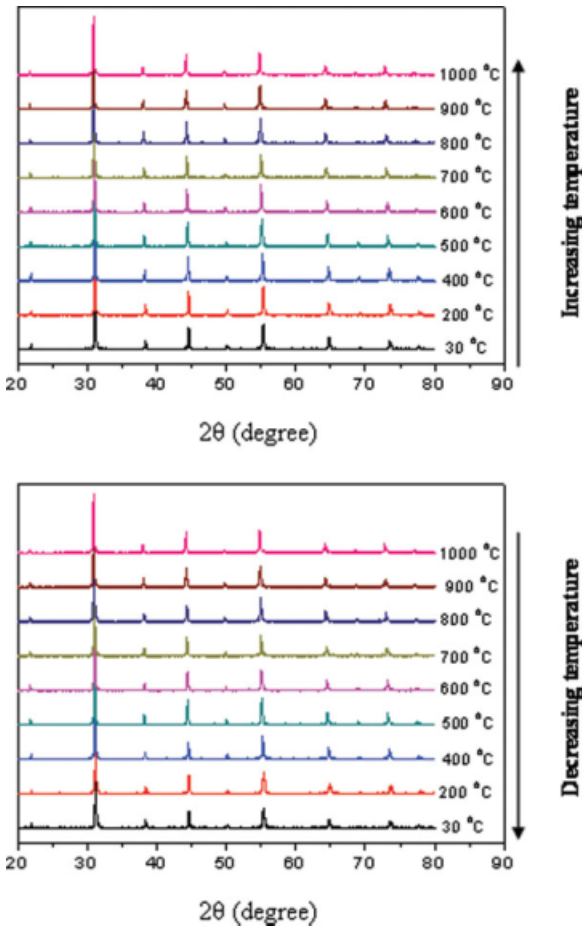

Figure 2. *In situ* XRD patterns of BCFT under air during increasing and decreasing temperatures.

Heating and cooling rate = 5°C/min, equilibration time at each temperature: 70 min for recording the XRD. [Color figure can be viewed in the online issue, which is available at www.interscience.wiley.com.]

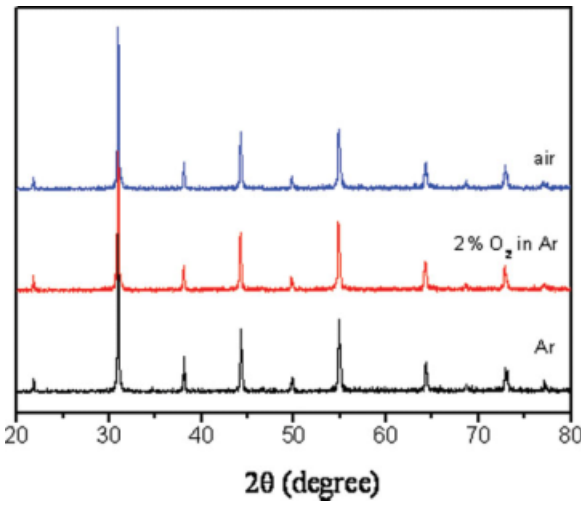

Figure 3. *In situ* XRD patterns of the BCFT under different atmospheres at 900°C.

Equilibration time: 70 min before recording XRD at each temperature. [Color figure can be viewed in the online issue, which is available at www.interscience.wiley.com.]

profiles of BCFT. As shown in Figure 5, two O_2 desorption peaks can be seen in the BCFT sample, one peak is between 250 and 500°C and the other between 830 and 1000°C. The low-temperature peak is attributed to the reduction of the high-valence states Fe^{4+} and/or Co^{4+} to Fe^{3+} and/or Co^{3+}. The high-temperature peak is attributed to the reduction of Fe^{3+} and/or Co^{3+} to Fe^{2+} and/or Co^{2+}. The reversibility of oxygen adsorption and desorption is a significant factor for a stable structure. The multirun O_2-TPD profiles in Figure 5 have the same profiles as the first-run one. It means that BCFT possesses good reversibility for the oxygen adsorption and desorption. After the multirun O_2-TPD, the sample is characterized by XRD, as shown in Figure 6. It can be seen that the perovskite structure was kept, which indicates that the BCFT exhibits an excellent structure stability and phase reversibility. The result is in agreement with the finding of *in situ* high-temperature XRD.

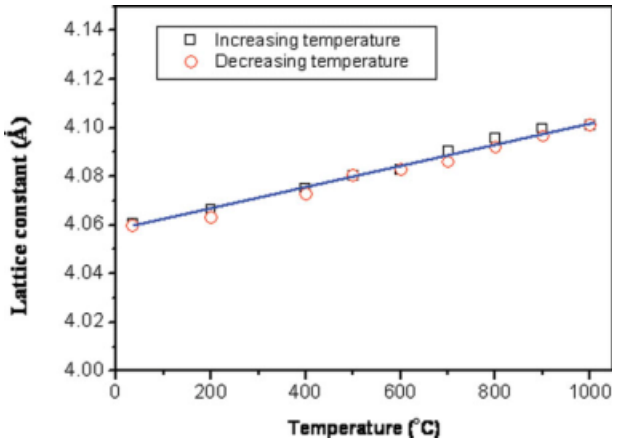

Figure 4. Temperature dependence of the lattice constants for BCFT.

[Color figure can be viewed in the online issue, which is available at www.interscience.wiley.com.]

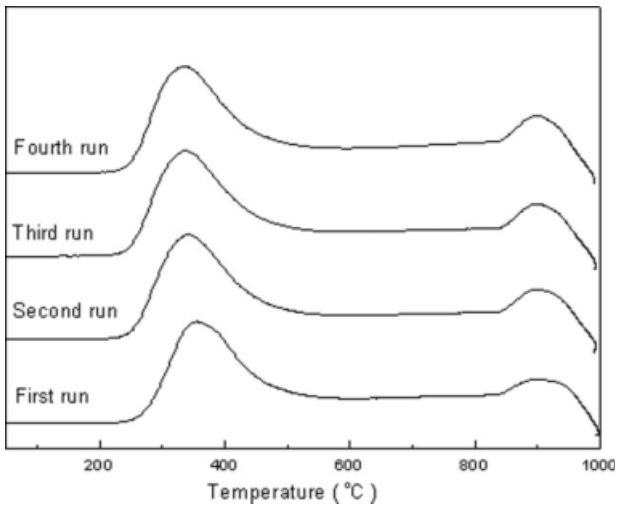

Figure 5. Multirun O_2-TPD profiles of the BCFT.

Good oxygen permeability is an important factor for the application of dense perovskite membranes and, therefore, the oxygen permeability of the BCFT membranes was investigated in detail. The oxygen permeation fluxes through the dense BCFT membranes of different thicknesses at different temperatures are presented in Figure 7. It can be seen that the oxygen permeation fluxes increase distinctly with increasing temperature. Furthermore, it can also be seen that the oxygen permeation fluxes increase remarkably with decreasing membrane thickness. The oxygen permeation flux through the membrane with a thickness of 1.2 mm was 1.05 ml/cm^2 min at the oxygen partial pressure of 0.021 bar on the sweep side, the J_{O2} through the membrane with a thickness of 0.60 mm can reach 2.22 ml/cm^2 min at the oxygen partial pressure of 0.043 bar on the sweep side. It is interesting to note that the J_{O2} through a membrane with a thickness of 1.0 mm was 1.58 ml/min cm^2 at 950°C, which is 1.8

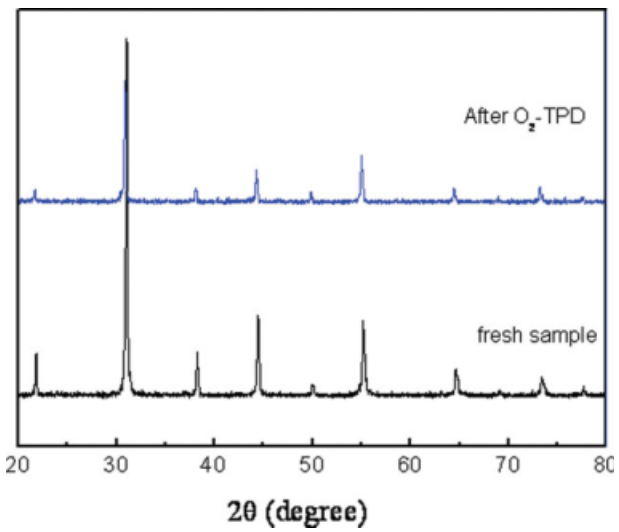

Figure 6. XRD patterns for the fresh BCFT and the sample after multirun O_2-TPD.

[Color figure can be viewed in the online issue, which is available at www.interscience.wiley.com.]

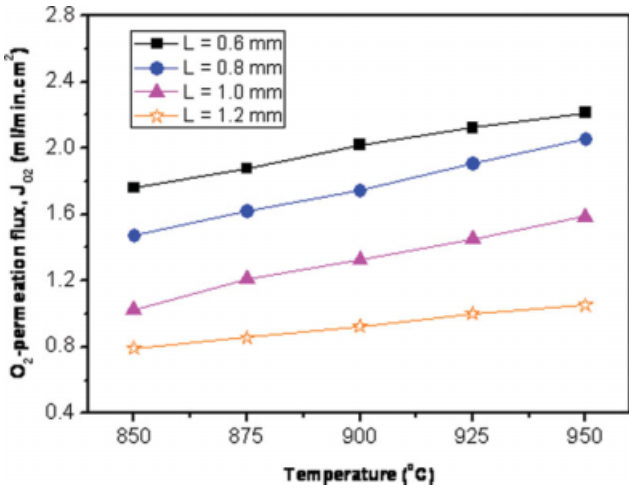

Figure 7. Temperature dependence of the oxygen permeation fluxes through BCFT membranes of different thicknesses.

[Color figure can be viewed in the online issue, which is available at www.interscience.wiley.com.]

times more than that through a BCFZ membrane (0.9 ml/min cm^2) at 950°C under a similar oxygen gradient as driving force (150 ml/min synthetic air, 30 ml/min He, thickness = 1.0 mm).[32]

If the bulk diffusion is the limiting step for the oxygen permeation, the oxygen permeation flux J_{O2} through the mixed electronic–ionic conducting membrane can be theoretically expressed by the following equation:

$$J_{O_2} = \frac{2.303RT\sigma_e\sigma_i}{16F^2(\sigma_e+\sigma_i)L}\log\frac{P_h}{P_l} \quad (3)$$

where R, F, T, and L denote the gas constant; Faraday constant; temperature; and thickness of the membrane, respectively. P_h and P_l are the oxygen partial pressures on the air and sweep sides. Note that the oxygen partial pressure on the sweep gas side depends on the oxygen permeation flux and the He flow rate. σ_e and σ_i are the electronic and ionic conductivity, respectively. Therefore, a plot of $J_{O_2}/\log\frac{P_h}{P_l}$ against the reciprocal of the membrane thickness ($1/L$) is linear and goes through the origin of the coordinates if the limiting step of the oxygen permeation is bulk diffusion. To determine the rate-limiting step of the oxygen permeation of BCFT, the oxygen permeation fluxes through membranes of different thickness were measured as a function of temperature. Figure 8 shows the plot of $J_{O_2}/\log\frac{P_h}{P_l}$ vs. the reciprocal of the membrane thickness at different temperatures. From Figure 8, it follows that the oxygen permeation fluxes increase linearly with $1/L$, which reveals that the overall oxygen permeation is limited by the bulk diffusion of the oxygen ions. The results demonstrate that a high-oxygen permeation flux for the commercial applications can be obtained by decreasing the membrane thickness such as via spinning the membrane in a hollow fiber configuration with an asymmetric structure.[1–6]

Figure 9 shows the oxygen permeation flux through the BCFT membrane as a function of time at 900°C. It was found that the oxygen permeation fluxes were steady during 120 h of operation. After the 120 hours' operation, both sides of the membrane were characterized by XRD. Figure 10 shows the XRD patterns of the membrane surface exposed to the air side and the He side. It was found that the membrane surface exposed to the He side kept the cubic perovskite structure, whereas on the membrane surface exposed to the air side some impurity peaks besides the cubic perovskite structure were found. We polished the membrane surface exposed to the air side several micrometers in depth, then XRD was used to characterize the structure. Only the cubic perovskite structure was observed, as shown in Figure 10. This finding indicates that the impurities were only on the membrane surface. EDXS analysis found around 3.82 atom% sulfur on the membrane surface exposed to the air side, most probably as $BaSO_4$. The sulfur stems were possibly from the traces of sulfur in the fed air. It should be pointed out that similar concentrations of sulfur on the perovskite membrane surface usually lead to a blockade of the oxygen permeability.[41] However, for BCFT membrane, it seems that the presence of sulfur has no significant poisoning influence on the oxygen permeability.

To demonstrate the stability of BCFT under a reducing atmosphere, a BCFT membrane was used to construct a reactor for the POM to syngas. The long-term POM reaction in a BCFT membrane reactor was performed at 900°C with 48% methane diluted by helium at the flow rate of 50 ml/min. A methane conversion of 99%, CO selectivity of 94%, and an oxygen permeation flux of around 16–17 ml/min cm^2 were achieved. The long-term time dependence of the oxygen permeation flux is shown in Figure 11. During the 400 h run, the oxygen permeation was fairly stable with a value of about 16.8 ml/ min cm^2, demonstrating the excellent performance of the membrane reactor. The excellent phase reversibility of the BCFT oxide might stabilize the membrane reactor under the highly reducing atmosphere, such as under synthesis gas conditions.

Conclusions

In this study, BCFT powders are synthesized in a solid state reaction. The results of *in situ* high-temperature XRD

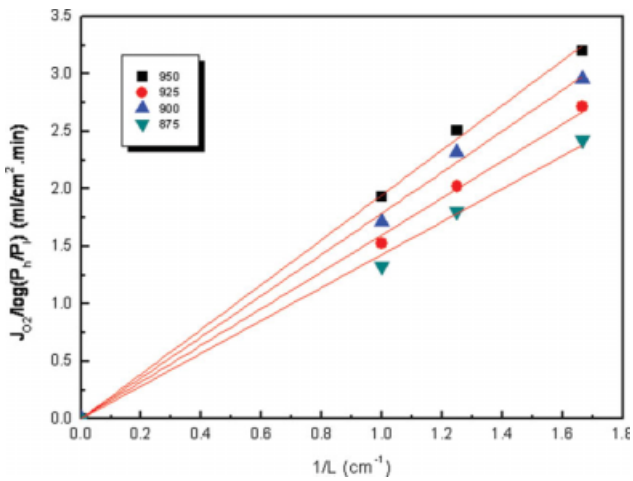

Figure 8. Relationship between oxygen permeation fluxes and the reciprocal thickness of BCFT membranes at different temperatures.

[Color figure can be viewed in the online issue, which is available at www.interscience.wiley.com.]

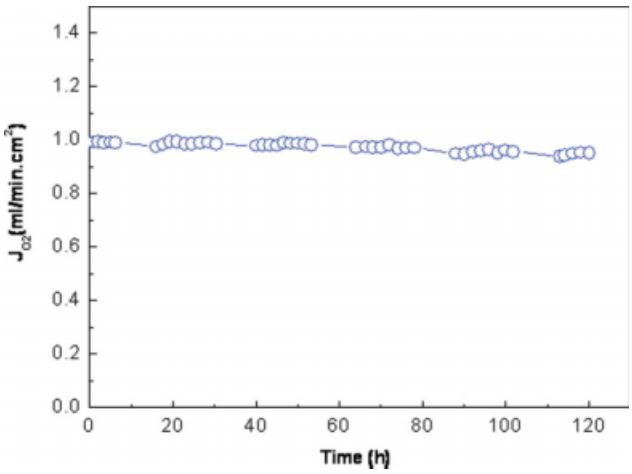

Figure 9. Oxygen permeation flux through BCFT as a function of time at 900°C.

Membrane thickness = 1.0 mm, air flow rate = 150 ml/min, He flow rate = 30 ml/min. [Color figure can be viewed in the online issue, which is available at www.interscience.wiley.com.]

and multirun O_2-TPD indicate that the BCFT membrane has good structure stability and phase reversibility in air at high temperatures. The thermal expansion coefficient (TEC) of $BaCo_{0.7}Fe_{0.2}Ta_{0.1}O_{3-\delta}$ of 1.02×10^{-5} K^{-1} is calculated from the *in situ* high-temperature XRD. It is found to be smaller than those of $Ba_{0.5}Sr_{0.5}Co_{0.8}Fe_{0.2}O_{3-\delta}$ (1.15×10^{-5} K^{-1}), $SrCo_{0.8}Fe_{0.2}O_{3-\delta}$ (1.79×10^{-5} K^{-1}), and $BaCo_{0.4}Fe_{0.4}Zr_{0.2}O_{3-\delta}$ (1.03×10^{-5} K^{-1}), which indicates that BCFT shows a good operation stability. Oxygen permeation fluxes are measured in the range of 850–950°C. Thickness dependence of oxygen permeation of the membrane indicates that oxygen permeation is controlled by bulk diffusion in the range of thicknesses of 0.6–1.2 mm. After 120 h oxygen permeation, it is found that the membrane surface exposed to the He side remains completely in the cubic

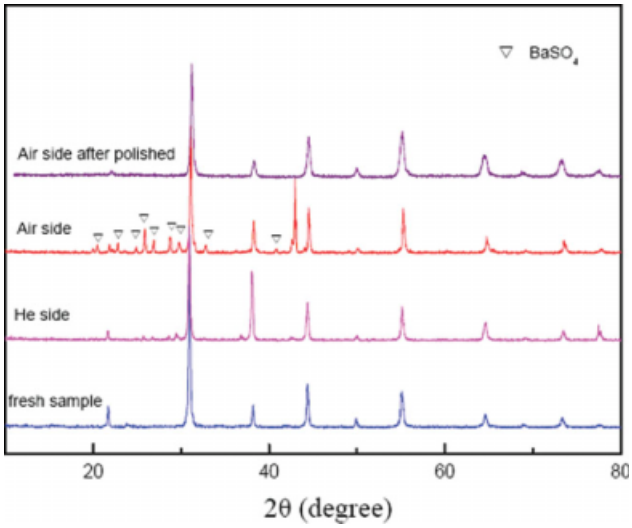

Figure 10. XRD patterns of the fresh and spent BCFT membranes.

[Color figure can be viewed in the online issue, which is available at www.interscience.wiley.com.]

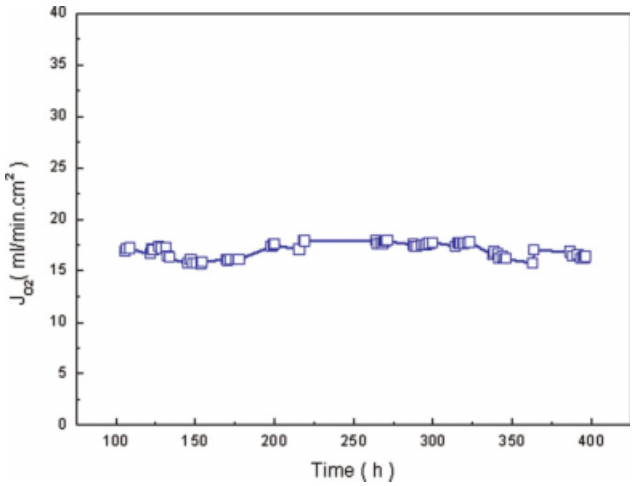

Figure 11. Long-term time dependence of oxygen permeation flux through BCFT membrane at 900°C under POM reaction conditions.

Sweep side: 48% methane diluted by He at a constant flow rate of 50 ml/min; air side: Air flow rate = 200 ml/min. 0.3 g Ni-based catalyst. [Color figure can be viewed in the online issue, which is available at www. interscience.wiley.com.]

structure while around 3.82 atom% sulfur are detected by EDXS on the membrane surface exposed to the synthetic air side, most probably as $BaSO_4$. Fortunately, the presence of sulfur has no significant effect on the oxygen permeability. A BCFT membrane reactor was successfully operated at 900°C for around 400 h in the POM reaction with fairly stable oxygen permeation flux of about 16.8 ml/min cm^2. The excellent phase reversibility of the material stabilized the membrane reactor under syngas atmosphere.

Acknowledgments

The authors greatly acknowledge the financial support by National Natural Science Foundation of China (nos. 20706020, U0834004), by Program for New Century Excellent Talents in University (no. NECT-07-0307), and by the National Basic Research Program of China (no. 2009CB623406).

Notation

$J_{N_2}^{Leak}$ = leaked nitrogen flux (ml/min cm^2)
$J_{O_2}^{Leak}$ = leaked oxygen flux (ml/min cm^2)
J_{O_2} = oxygen permeation flux (ml/min cm^2)
C_{O_2} = oxygen concentration (%)
C_{N_2} = nitrogen concentration (%)
f = total flow rate of the outlet on the sweep side (ml/min)
S = membrane area (cm^2)
a = lattice constant (Å)
a_0 = lattice constant at room temperature (Å)
P_h = oxygen partial pressures on the air side (bar)
P_l = oxygen partial pressure the sweep side (bar)
P_o = standard pressure (P_o = 1 bar)
R = gas constant (R = 8.3145 J/mol K)
F = Faraday constant (C/mol)
T = temperature (°C)
L = thickness of the membrane (mm)

Greek letters

δ = oxygen nonstoichiometry, $0 < \delta < 1$
σ_i = ion conductivity (S/m)
σ_e = electronic conductivity (S/m)

Literature Cited

1. Liu SM, Tan XY, Shao ZP, da Costa JCD. $Ba_{0.5}Sr_{0.5}Co_{0.8}Fe_{0.2}O_{3-\delta}$. ceramic hollow-fiber membranes for oxygen permeation. *AIChE J*. 2006;52:3452.
2. Liu SM, Gavalas GR. Oxygen selective ceramic hollow fiber membranes. *J Memb Sci*. 2005;246:103.
3. Tan XY, Liu Y, Li K. Mixed conducting ceramic hollow-fiber membranes for air separation. *AIChE J*. 2005;51:1991.
4. Tan XY, Liu Y, Li K. Preparation of LSCF ceramic hollow-fiber membranes for oxygen production by a phase-inversion/sintering technique. *Ind Eng Chem Res*. 2005;44:61.
5. Tan XY, Li K. Oxygen production using dense ceramic hollow fiber membrane modules with different operating modes. *AIChE J*. 2007;53:838.
6. Wang HH, Werth S, Schiestel T, Caro J. Perovskite hollow-fiber membranes for the production of oxygen-enriched air. *Angew Chem Int Ed*. 2005;44:2.
7. Xu NP, Li SG, Jin WQ, Shi J, Lin YS. Experimental and modeling study on tubular dense membranes for oxygen permeation. *AIChE J*. 1999;45:2519.
8. Vente JF, Haije WG, Rak ZS. Performance of functional perovskite membranes for oxygen production. *J Memb Sci*. 2006;276:178.
9. Wu ZT, Jin WQ, Xu NP. Oxygen permeability and stability of Al_2O_3-doped $SrCo_{0.8}Fe_{0.2}O_{3-\delta}$ mixed conducting oxides. *J Memb Sci*. 2006;279:320.
10. Vente JF, Haije WG, Rak ZS. Performance of functional perovskite membranes for oxygen production. *J Memb Sci*. 2006;276:178.
11. Balachandran U, Dusek JT, Maiya PS, Ma B, Mieville RL, Kleefisch MS, Udovich CA. Ceramic membrane reactor for converting methane to syngas. *Catal Today*. 1997;36:265.
12. Gu XH, Jin WQ, Chen CL, Xu NP, Shi J, Ma YH. YSZ-$SrCo_{0.4}$-$Fe_{0.6}O_{3-\delta}$ membranes for the partial oxidation of methane to syngas. *AIChE J*. 2002;48:2051.
13. Chen CS, Feng SJ, Ran S, Zhu DC, Liu W, Bouwmeester HJM. Conversion of methane to syngas by a membrane-based oxidation-reforming process. *Angew Chem Int Ed*. 2003;42:5196.
14. Wang HH, Feldhoff A, Schiestel T, Werth S, Caro J. Oxygen selective ceramic hollow fiber membranes for POM. *AIChE J*. Available online in Wiley Interscience, DOI: 10.1002/aic.11856.
15. Jiang HQ, Wang HH, Werth S, Schiestel T, Caro J. Simultaneous production of hydrogen and synthesis gas by combining water splitting with partial oxidation of methane in a hollow fiber membrane reactor. *Angew Chem Int Ed*. 2008;47:9341.
16. Jiang HQ, Wang HH, Liang FY, Werth S, Schiestel T, Caro J. Direct decomposition of nitrous oxide to nitrogen by in-situ oxygen removal with a perovskite membrane. *Angew Chem Int Ed*. 2009; 48:2983.
17. Wang HH, Cong Y, Yang WS. High selectivity of oxidative dehydrogenation of ethane to ethylene in an oxygen permeable membrane reactor. *Chem Commun*. 2002;14:1468.
18. Rebeilleau-Dassonneville M, Rosini S, van Veen AC, Farrusseng D, Mirodatos C. Oxidative activation of ethane on catalytic modified dense ionic oxygen conducting membranes. *Catal Today*. 2005;104:131.
19. Akin FT, Lin YS. Selective oxidation of ethane to ethylene in a dense tubular membrane reactor. *J Memb Sci*. 2002;209:457.
20. Ren JY, Fan YQ, Egolfopoulos FN, Tsotsis TT. Membrane-based reactive separations for power generation applications: oxygen lancing. *Chem Eng Sci*. 2003;58:1043.
21. Fan YQ, Ren JY, Onstot W, Pasale J, Tsotsis TT, Egolfopoulos FN. Reactor and technical feasibility aspects of a CO_2 decomposition-based power generation cycle, utilizing a high-temperature membrane reactor. *Ind Eng Chem Res*. 2003;42:2618.
22. Teraka Y, Zhang HM, Furukawa S, Minra N, Yamazoe N. Oxygen permeation through pervoskite-type oxides. *Chem Lett*. 1985;14: 1743.
23. Wang HH, Cong Y, Yang WS. Investigation on the partial oxidation of methane to syngas in a tubular $Ba_{0.5}Sr_{0.5}Co_{0.8}Fe_{0.2}O_{3-\delta}$ membrane reactor. *Catal Today*. 2003;82:157.
24. Shao ZP, Dong H, Xiong GX, Cong Y, Yang WS. Performance of a mixed-conducting ceramic membrane reactor with high oxygen permeability for methane conversion. *J Memb Sci*. 2001;183:181.
25. Tong JH, Yang WS, Cai R, Zhu BC, Xiong GX, Lin LW. Investigation on the structure stability and oxygen permeability of titanium-doped perovskite-type oxides of $BaTi_{0.2}Co_xFe_{0.8-x}O_{3-\delta}$($x=_{0.2-0.6}$). *Separ Purif Technol*. 2003;32:289.
26. Lu H, Deng ZQ, Tong JH, Yang WS. Oxygen permeability and structural stability of Zr-doped oxygen-permeable $Ba_{0.5}Sr_{0.5}Co_{0.8}$-$Fe_{0.2}O_{3-\delta}$ membrane. *Mater Lett*. 2005;59:2285.
27. Lu H, Tong JH, Deng ZQ, Cong Y, Yang WS. Crystal structure, oxygen permeability and stability of $Ba_{0.5}Sr_{0.5}Co_{0.8}Fe_{0.1}M_{0.1}O_{3-\delta}$(M = Fe, Cr, Mn, Zr) oxygen-permeable membranes. *Mater Res Bull*. 2006;41:683.
28. Gu XH, Jin WQ, Chen CL, Xu NP, Shi J, Ma YH. YSZ-$SrCo_{0.4}$-$Fe_{0.6}O_{3-\delta}$ membranes for the partial oxidation of methane to syngas. *AIChE J*. 2002;48:2051.
29. Kharton VV, Tsipis EV, Marozau IP, Yaremchenko AA, Valente AA, Viskup AP, Frade JR, Naumovich EN, Rocha J. Transport and electrocatalytic properties of $La_{0.3}Sr_{0.7}Co_{0.8}Ga_{0.2}O_{3-\delta}$ membranes. *J Solid State Electrochem*. 2005;9:10.
30. Shaula AL, Kharton VV, Patrakeev MV, Waerenborgh JC, Rojas DP, Marques FMB. Defect formation and transport in $SrFe_{1-x}Al_xO_{3-\delta}$. *Ionics*. 2004;10:378.
31. Shaula AL, Kharton VV, Vyshatko NP, Tsipis EV, Patrakeev MV, Marques FMB, Frade JR. Oxygen ionic transport in $SrFe_{1-y}$ $Al_yO_{3-\delta}$ and $Sr_{1-x}Ca_xFe_{0.5}Al_{0.5}O_{3-\delta}$ ceramics. *J Eur Ceram Soc*. 2005;25:489.
32. Tong JH, Yang WS, Zhu BC, Cai R. Investigation of ideal zirconium-doped perovskite-type ceramic membrane materials for oxygen separation. *J Memb Sci*. 2002;203:175.
33. Wang HH, Tablet C, Feldhoff A, Caro J. A cobalt-free oxygen-permeable membrane based on the perovskite-type oxide $Ba_{0.5}Sr_{0.5}$ $Fe_{0.8}Zn_{0.2}O_{3-\delta}$. *Adv Mater*. 2005;17:1785.
34. Zeng PY, Ran R, Chen ZH, Gu HX, Shao ZP, Liu SM. Novel mixed conducting $SrSc_{0.05}Co_{0.95}O_{3-\delta}$, ceramic membrane for oxygen separation. *AIChE J*. 2007;53:3116.
35. Zeng PY, Ran R, Chen ZH, Zhou W, Gu HX, Shao ZP, Liu SM. Efficient stabilization of cubic perovskite $SrCoO_{3-\delta}$ by B-site low concentration scandium doping combined with sol-gel synthesis. *J Alloy Comp*. 2008;455:465.
36. Nagai T, Ito W, Sakon T. Relationship between cation substitution and stability of perovskite structure in $SrCoO_{3-\delta}$ based mixed conductors. *Solid State Ionics*. 2007;177:3433.
37. Shao ZP, Yang WS, Cong Y, Dong H, Tong JH, Xiong GX. Investigation of the permeation behaviour and stability of a $Ba_{0.5}Sr_{0.5}Co_{0.8}$ $Fe_{0.2}O_3$ oxygen membrane. *J Memb Sci*. 2000;172:177.
38. Makoto H, Kazunari D, Michhikazu H, Takashi T. $Ba_{1.0}Co_{0.7}$ $Fe_{0.2}Nb_{0.1}O_{3-\delta}$ dense ceramic as an oxygen permeable membrane for partial oxidation of methane to synthesis gas. *Chem Lett*. 2006;35:1326.
39. Cheng YF, Zhao HL, Teng DQ, Li FS, Lu XG, Ding WZ. Investigation of Ba fully occupied A-site $BaCo_{0.7}Fe_{0.3-x}Nb_xO_{3-\delta}$ perovskite stabilized by low concentration of Nb for oxygen permeation membrane. *J Memb Sci*. 2008;322:484.
40. Wang HH, Tablet C, Yang WS, Caro J. In situ high temperature X-ray diffraction studies of mixed ionic and electronic conducting perovskite-type oxides. *Mater Lett*. 2005;59:3750.
41. Wang HH, Schiestel T, Tablet C, Schroeder M, Caro J. Mixed oxygen ion and electron conducting hollow fiber membranes for oxygen separation. *Solid State Ionics*. 2006;177:2255.

Manuscript received May 26, 2009, and revision received July 17, 2009.